

Indirect detection prospects for $d^*(2380)$ dark matter

Geoff Beck

School of Physics, University of the Witwatersrand, Private Bag 3, WITS-2050,
Johannesburg, South Africa

E-mail: geoffrey.beck@wits.ac.za

March 2020

Abstract. A Bose-Einstein condensate of the hexaquark particle known as $d^*(2380)$ has been recently proposed as a dark matter candidate by the authors in Bashkanov & Watts 2020. This particle can produced in an abundant condensate state in the early universe and is argued to satisfy all the stability and weak interaction constraints of a viable dark matter candidate. This dark matter candidate is able to evade direct detection bounds and is suggested to have the best observational prospects in the form of indirect astrophysical emissions due to the decay of the d^* condensate. In this work we test the indirect observational prospects of this form of dark matter and find that its low mass ~ 2 GeV mean that sub-GeV gamma-rays searches have the best prospects in the Milky-Way galactic centre where we find $\Gamma_{d^*} < 3.9 \times 10^{-24} \text{ s}^{-1}$, with current extra-galactic data from M31 and the Coma cluster producing constraints on the d^* decay rate two orders of magnitude weaker.

Keywords: dark matter, hexaquarks

Submitted to: *J. Phys. G: Nucl. Part. Phys.*

1. Introduction

The nature of Dark Matter (DM) remains one of the most important problems in astroparticle physics. Despite extensive gravitational evidence [1] neither direct [2] nor indirect searches [1, 3, 4] have produced anything beyond parameter space constraints. In particular the direct detection experiments have strongly narrowed the space of viable supersymmetric Weakly Interacting Massive Particles (WIMPs) [2]. A recent proposal of new form of light quark based DM consists of having the hexaquark particle $d^*(2380)$ formed in the early universe and existing until the present epoch in the form of a stable Bose-Einstein Condensate (BEC) [5].

The authors in [5] argue that the most probable signature of this form of DM is likely to come from astrophysical emissions from the decay of the d^* BEC. In this letter

we explore the potential of indirect observations to detect the signatures of d^* decay in both radio and gamma-ray frequencies. Our findings are that the best extra-galactic target constraint on the decay rate was from the M31 galaxy with $\Gamma_{d^*} < \times 10^{-22} \text{ s}^{-1}$ which corresponds to lower limit on the d^* BEC lifetime several orders of magnitude longer than the age of the universe [6]. A model independent search in diffuse galactic gamma-rays from [7] found $\Gamma < 10^{-24} \text{ s}^{-1}$ but the photon yield per decay in this model exceeds the hexaquark case from [5] by 5 orders of magnitude at energies around 0.1 GeV where our constraints are derived. So we exceed a ‘model-translated’ version of the [7] limit by two orders of magnitude in extra-galactic targets.

In our own galactic centre we find the strongest observational prospect. Using the CLUMPY software [28, 29, 30] to determine a dark matter halo density profile we find that $\Gamma_{d^*} < 3.9 \times 10^{-24}$, a full two order of magnitude improvement on extra-galactic data. The galactic centre gamma-ray data set we used was for the Fermi-LAT GeV excess spectrum from [34] as this d^* decay contributes to anomalous emissions not covered by the Fermi templates. The use of this spectrum greatly improves constraints as the flux is at least an order of magnitude below the total signal observed by Fermi-LAT. These limits better the translated limits from [7] by 5 orders of magnitude and are competitive with the unmodified limits on light DM decay via electrons with final-state radiation (we compare to this case as its spectral shape is most similar to the d^* data from [5]).

This letter is structured as follows: in section 2 the particle distribution functions from d^* decays are discussed with the emission mechanisms then detailed in sections 3, 4, and 5. The DM target halos are described in 6 and the observational flux data for these targets is listed in 7. The results are presented in section 8 and conclusions are drawn and discussed in section 9.

2. $d^*(2380)$ decay particle source functions

The source function for particle species i is found according to

$$Q_i(r, E) = \Gamma_{d^*} \frac{dN_i}{dE} \left(\frac{\rho_{d^*}(r)}{m_{d^*}} \right), \quad (1)$$

where Γ_{d^*} is the decay rate, $\frac{dN_i}{dE}$ is the particle number per unit energy from a d^* decay, ρ_{d^*} is the DM density, and $m_{d^*} = 0.238 \text{ GeV}$.

The yield functions $\frac{dN_i}{dE}$ for photons are drawn directly from results presented in [5]. However, in the case of the electron yield function the calculation is more involved. The authors in [5] present yields for π^\pm but not e^\pm . Thus, to obtain the latter we convert the pion distributions to those of electrons/positrons following [8] which notably omits radiative corrections.

3. High-energy emissions from d^* decay

We will look at three mechanisms for high-energy emissions: Inverse-Compton Scattering (ICS), bremsstrahlung, and more direct gamma-ray emission. The power produced by the ICS at a photon of frequency ν from an electron with energy E is given by [9, 10]

$$P_{IC}(\nu, E, z) = cE_\gamma(z) \int d\epsilon n(\epsilon) \sigma(E, \epsilon, E_\gamma(z)) , \quad (2)$$

where $E_\gamma(z) = h\nu(1+z)$, ϵ is the energy of the seed photons distributed according to $n(\epsilon)$, and

$$\sigma(E, \epsilon, E_\gamma) = \frac{3\sigma_T}{4\epsilon\gamma^2} G(q, \Gamma_e) , \quad (3)$$

with σ_T being the Thompson cross-section and

$$G(q, \Gamma_e) = 2q \ln q + (1+2q)(1-q) + \frac{(\Gamma_e q)^2(1-q)}{2(1+\Gamma_e q)} , \quad (4)$$

with

$$q = \frac{E_\gamma}{\Gamma_e(\gamma m_e c^2 + E_\gamma)} , \quad (5)$$

$$\Gamma_e = \frac{4\epsilon\gamma}{m_e c^2} ,$$

where m_e is the electron mass.

The power from bremsstrahlung at photon energy E_γ from an electron at energy E is given by [9, 10]

$$P_B(E_\gamma, E, r) = cE_\gamma(z) \sum_j n_j(r) \sigma_B(E_\gamma, E) , \quad (6)$$

n_j is the distribution of target nuclei of species j , the cross-section is given by

$$\sigma_B(E_\gamma, E) = \frac{3\alpha\sigma_T}{8\pi E_\gamma} \left[\left(1 + \left(1 - \frac{E_\gamma}{E} \right)^2 \right) \phi_1 - \frac{2}{3} \left(1 - \frac{E_\gamma}{E} \right) \phi_2 \right] , \quad (7)$$

with ϕ_1 and ϕ_2 being energy dependent factors determined by the species j (see [9, 10]).

The emissivity of mechanism i (ICS or bremsstrahlung) is given by

$$j_i(\nu, r, z) = \int_{m_e}^{M_\chi} dE \left(\frac{dn_{e^-}}{dE} + \frac{dn_{e^+}}{dE} \right) P_i(\nu, E, r, z) , \quad (8)$$

where $\frac{dn_{e^\pm}}{dE}$ is the electron distribution within the source region from d^* decay. The flux is then found via

$$S_i(\nu, z) = \int_0^r d^3r' \frac{j_i(\nu, r', z)}{4\pi(D_L^2 + (r')^2)} , \quad (9)$$

where D_L is the luminosity distance to the halo centre.

The flux from more direct photon production is found simply via

$$S_\gamma(\nu, z) = \int_0^r d^3r' \frac{Q_\gamma(\nu, z, r)}{4\pi(D_L^2 + (r')^2)}, \quad (10)$$

where Q_γ is the gamma-ray source function.

4. Radio emissions from d^* decay

The power from synchrotron emission at frequency ν from electron at energy E is given by [10, 9]

$$P_{synch}(\nu, E, r, z) = \int_0^\pi d\theta \frac{\sin \theta}{2} 2\pi \sqrt{3} r_e m_e c \nu_g F_{synch} \left(\frac{\kappa}{\sin \theta} \right), \quad (11)$$

where m_e is the electron mass, $\nu_g = \frac{eB}{2\pi m_e c}$ is the non-relativistic gyro-frequency, $r_e = \frac{e^2}{m_e c^2}$ is the classical electron radius, and the quantities κ and F_{synch} are defined as

$$\kappa = \frac{2\nu(1+z)}{3\nu_g \gamma^2} \left[1 + \left(\frac{\gamma \nu_p}{\nu(1+z)} \right)^2 \right]^{\frac{3}{2}}, \quad (12)$$

with the plasma frequency $\nu_p \propto \sqrt{n_e}$, γ as the electron Lorentz factor, and

$$F_{synch}(x) = x \int_x^\infty dy K_{5/3}(y) \approx 1.25 x^{\frac{1}{3}} e^{-x} (648 + x^2)^{\frac{1}{12}}. \quad (13)$$

The flux is found in the same manner as ICS and bremsstrahlung, following equations (8) and (9) using P_{synch} .

5. Electron equilibrium distributions

The synchrotron, ICS, and bremsstrahlung mechanisms require the spectrum of electrons injected via DM decays. This will be taken to be the equilibrium solution to the diffusion equation

$$\frac{\partial}{\partial t} \frac{dn_e}{dE} = \nabla \cdot \left(D(E, \mathbf{r}) \nabla \frac{dn_e}{dE} \right) + \frac{\partial}{\partial E} \left(b(E, \mathbf{r}) \frac{dn_e}{dE} \right) + Q_e(E, \mathbf{r}), \quad (14)$$

where method of solution is to assume the diffusion and energy-loss functions D and b have no position dependence, such that

$$D(E) = D_0 \left(\frac{d_0}{1 \text{ kpc}} \right)^{\frac{2}{3}} \left(\frac{\bar{B}}{1 \mu\text{G}} \right)^{-\frac{1}{3}} \left(\frac{E}{1 \text{ GeV}} \right)^{\frac{1}{3}}, \quad (15)$$

where $D_0 = 3.1 \times 10^{28} \text{ cm}^2 \text{ s}^{-1}$, d_0 is the magnetic field coherence length, \bar{B} is the average magnetic field strength, and E is the electron energy. The loss-function is

found via [11, 12]

$$b(E) = b_{IC} \left(\frac{E}{1 \text{ GeV}} \right)^2 + b_{sync} \left(\frac{E}{1 \text{ GeV}} \right)^2 \bar{B}^2 + b_{Coul} \bar{n} \left(1 + \frac{1}{75} \log \left(\frac{\gamma}{\bar{n}} \right) \right) + b_{brem} \bar{n} \left(\frac{E}{1 \text{ GeV}} \right), \quad (16)$$

where \bar{n} is the average gas density, the coefficients b_{IC} , b_{sync} , b_{Coul} , b_{brem} are the energy-loss rates from ICS, synchrotron emission, Coulomb scattering, and bremsstrahlung. These coefficients are given by $0.25 \times 10^{-16}(1+z)^4/6.08 \times 10^{-16}$ (for CMB/inter-stellar radiation fields), 0.0254×10^{-16} , 6.13×10^{-16} , 4.7×10^{-16} in units of GeV s^{-1} .

The solution used follows the methods outlined in [11] similar to [13, 14]. Full details can be found in [15]. It should be noted that, to better reflect the environment of the decays, the average values \bar{B} , \bar{n} are weighted by the halo DM density.

6. Halo environments

The primary halo characteristic is the DM density profile, we will make use of the Navarro-Frenk-White (NFW) case [16], the cored Burkert profile [17], and the Einasto profile [31]

$$\begin{aligned} \rho_{nfw}(r) &= \frac{\rho_s}{\left(\frac{r}{r_s} \left(1 + \frac{r}{r_s} \right) \right)^2}, \\ \rho_{burk}(r) &= \frac{\rho_s}{\left(1 + \frac{r}{r_s} \right) \left(1 + \left[\frac{r}{r_s} \right]^2 \right)}, \\ \rho_{ein}(r) &= \rho_s \exp \left[-\frac{2}{\alpha} \left(\left[\frac{r}{r_s} \right]^\alpha - 1 \right) \right], \end{aligned} \quad (17)$$

where α is the Einasto parameter, while r_s and ρ_s are the characteristic halo scale and density respectively.

6.1. Coma

In the Coma galaxy cluster we follow [11] in using the halo parameters $M_{vir} = 1.33 \times 10^{15} M_\odot$, $R_{vir} = 1.96 \text{ Mpc}$, and $r_s = 0.196 \text{ Mpc}$ with an NFW profile (ρ_s is chosen to normalise the density to M_{vir} within R_{vir}).

The gas density within the halo is taken to have a profile

$$n_e(r) = n_0 \left(1 + \left[\frac{r}{r_d} \right]^2 \right)^{-q_e}, \quad (18)$$

with $n_0 = 3.44 \times 10^{-3} \text{ cm}^{-3}$, $q_e = 1.125$, $r_d = 0.29 \text{ Mpc}$ from [18].

The magnetic field model is then

$$B(r) = B_0 \left(\frac{n_e(r)}{n_0} \right)^{q_b}, \quad (19)$$

with $B_0 = 4.7 \text{ } \mu\text{G}$, and $q_b = 0.5$ from [19].

6.2. M31

In M31 we will use an NFW profile with parameters found in [20] to be $M_{vir} = 1.04 \times 10^{12} M_\odot$, $R_{vir} = 0.207$ Mpc, and $r_s = 0.0167$ Mpc (ρ_s is chosen to normalise the density to M_{vir} within R_{vir}). In M31 we use an exponential gas density

$$n_e(r) = n_0 \exp\left(-\frac{r}{r_d}\right), \quad (20)$$

with $n_0 = 0.06 \text{ cm}^{-3}$ [21], and $r_d \approx 5$ kpc fitted in [22]. In this environment we use the magnetic field model from [22] which has, within $r \leq 40$ kpc,

$$B(r) = \frac{4.6 \left(\frac{r_1}{1 \text{ kpc}}\right) + 64}{\left(\frac{r_1}{1 \text{ kpc}}\right) + \left(\frac{r}{1 \text{ kpc}}\right)} \mu\text{G}, \quad (21)$$

with $r_1 = 200$ kpc.

6.3. Reticulum II

The Reticulum II dwarf galaxy is taken to have a Burkert density profile following arguments from [23, 24]. This profile has $r_s = 0.139$ kpc [25] and is normalised to the annihilation J-factor $8 \times 10^{18} \text{ GeV}^2 \text{ cm}^{-5}$ found in [4] within 0.5° of the galaxy centre.

In Reticulum II we follow [25] in using the profiles for gas density and magnetic field strength:

$$n_e(r) = n_0 \exp\left(-\frac{r}{r_d}\right), \quad (22)$$

and

$$B(r) = B_0 \exp\left(-\frac{r}{r_d}\right). \quad (23)$$

We take r_d to be given by the stellar-half-light radius with a value of 15 pc [26, 27] and we assume $B_0 \approx 1 \mu\text{G}$, $n_0 \approx 10^{-6} \text{ cm}^{-3}$.

6.4. Galactic centre

We use only the gamma-ray spectrum in the galactic centre and so our model data consist of just the annihilation J-factor. This we find using CLUMPY [28, 29, 30] to be $9.94 \times 10^{22} \text{ GeV}^2 \text{ cm}^{-5}$ within 10° of the galactic centre assuming an Einasto halo profile. We normalise our halo profile to the stated J-factor (using the CLUMPY halo parameters) in order to determine the decay products from this target.

7. Target environment fluxes

In the Coma galaxy cluster we make use of the diffuse radio data set from [32] and the gamma-ray limits from [3]. For M31 we make use of the radio frequency data set

from [15], these are divided into 50' and 15' observing regions (see [15] and references therein for further details). For gamma-rays in M31 we use the data points (but not upper-limits at higher energies) from [33]. In Reticulum II we use the diffuse flux limit of $12 \mu\text{Jy}$ at 1.873 GHz from [25], and the gamma-ray upper-limits from [4]. To follow [7] we test the gamma-ray spectrum of the Fermi-LAT excess from [34] against DM predictions using the 10° region of interest around the galactic centre.

8. Results

We display predicted spectra assuming $\Gamma_{d^*} = 10^{-24} \text{ s}^{-1}$ noting that largely model independent constraints for DM decaying to photons in [7] find that $\Gamma < 10^{-24} \text{ s}^{-1}$. The limits from [7] are not completely compatible with the model from [5]. This is because, while the spectral shapes are somewhat similar, the model-independent gamma-ray yields are around 5 orders of magnitude larger than those presented for the decay of d^* particles. So a rough benchmark to compare with our limits derived here will be $\Gamma_{d^*} < 10^{-19} \text{ s}^{-1}$. Additionally, this makes a reasonable benchmark due to the similarity of this $1/\Gamma_{d^*}$ to the age of the universe [6].

In the case of the Coma galaxy cluster in Figure 1 it is evident that existing gamma-ray upper-limits provide the strongest option for constraint in this environment with $\Gamma_{d^*} \leq 7.4 \times 10^{-22} \text{ s}^{-1}$ to avoid exceeding the limits at 2σ confidence interval. The observed radio data points are at least 5 orders of magnitude above the predicted spectrum. The resulting constraints from this data are $\Gamma_{d^*} \leq 3.6 \times 10^{-17} \text{ s}^{-1}$. Our results in the Coma case already exceed the model-translated galactic diffuse case from [7] by around 2 orders of magnitude.

M31 results are displayed in Figs. 2 and 3 are also well below the observed data points for the fiducial Γ value. However, the gamma-ray data points from [33] provide a constraint that $\Gamma_{d^*} \leq 1.2 \times 10^{-22} \text{ s}^{-1}$ at the 2σ confidence level. This is vastly better than the Coma cluster radio constraint, and a factor of 6 or so better than the gamma-ray case. Substantially weaker limits result from the radio data points, largely as the synchrotron emissions peak at such a low frequency as a consequence of the $\sim 2 \text{ GeV}$ d^* mass.

In Figure 4 we display the Reticulum II predicted spectrum. Importantly, the gamma-ray data points do not overlap with the predicted spectrum so can provide no constraints. However, the steep gamma-ray peak suggests that lower energy observations could provide a relatively strong probe of d^* decays in this target. If the power-law trend of the limits is continued, a $\Gamma_{d^*} \leq 10^{-23} \text{ s}^{-1}$ is potentially attainable, bettering even the M31 case. The relatively low energy threshold for ICS dominance in the Reticulum II spectrum also produces surprisingly strong radio limits with $\Gamma_{d^*} \leq 1.04 \times 10^{-14} \text{ s}^{-1}$.

In figure 5 we display the case of the galactic centre gamma-ray spectrum compared to the data from the Fermi-LAT diffuse gamma-ray excess within 10° from [34]. Here we see that the $\Gamma_{d^*} = 10^{-24} \text{ s}^{-1}$ case only lies slightly below the observed spectrum and a resulting constraint is that $\Gamma_{d^*} \leq 3.9 \times 10^{-24} \text{ s}^{-1}$, improving on the model translated

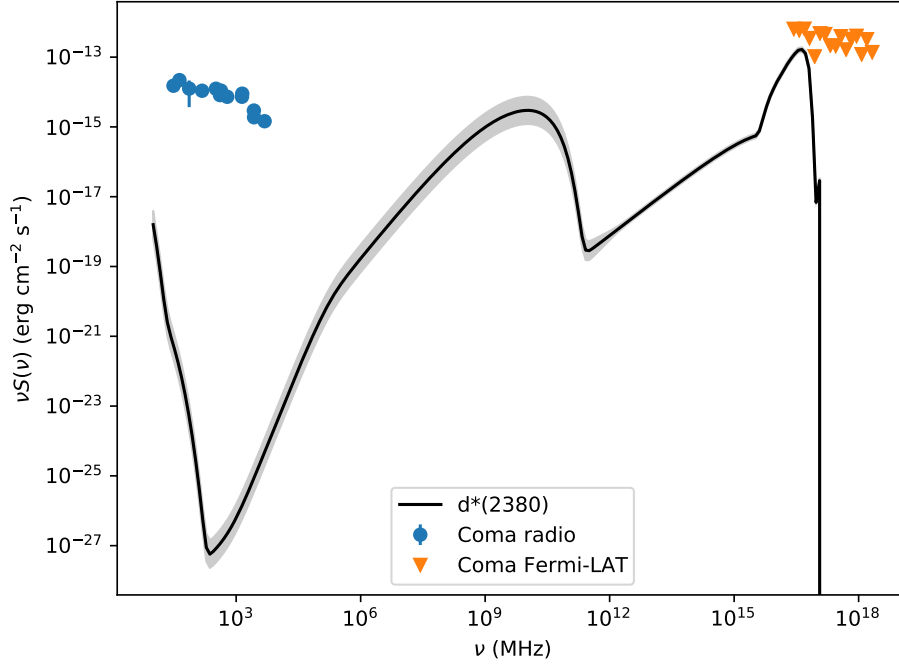


Figure 1. Predicted multi-frequency spectrum from d^* decay in the Coma galaxy cluster with $\Gamma_{d^*} = 10^{-24} \text{ s}^{-1}$. The shaded region indicates uncertainties from the magnetic field and halo mass.

value from [7] by around 5 orders of magnitude making this competitive even with the unmodified model independent limits.

9. Discussion and conclusions

We present here a summary of the constraints on the d^* decay rate Γ_{d^*} in 1 These results

Data set	Limit
GC gamma-ray	$\Gamma_{d^*} \leq 3.9 \times 10^{-24} \text{ s}^{-1}$
M31 gamma-ray	$\Gamma_{d^*} \leq 1.2 \times 10^{-22} \text{ s}^{-1}$
Coma gamma-ray	$\Gamma_{d^*} \leq 7.4 \times 10^{-22} \text{ s}^{-1}$
Coma radio	$\Gamma_{d^*} \leq 3.6 \times 10^{-17} \text{ s}^{-1}$
Reticulum II radio	$\Gamma_{d^*} \leq 1.04 \times 10^{-14} \text{ s}^{-1}$
M31 radio	$\Gamma_{d^*} \leq 4.9 \times 10^{-14} \text{ s}^{-1}$

Table 1. Summary of 2σ confidence interval limits on the d^* decay rate in different DM halos.

indicate that the various fluxes from d^* decay are weak but benchmarking against the viability of the hexaquark DM model is difficult without a result for Γ which would be necessary to reproduce the present-day DM abundance. The most comparable limit is the largely model independent set from [7] which uses diffuse X-ray and gamma-ray

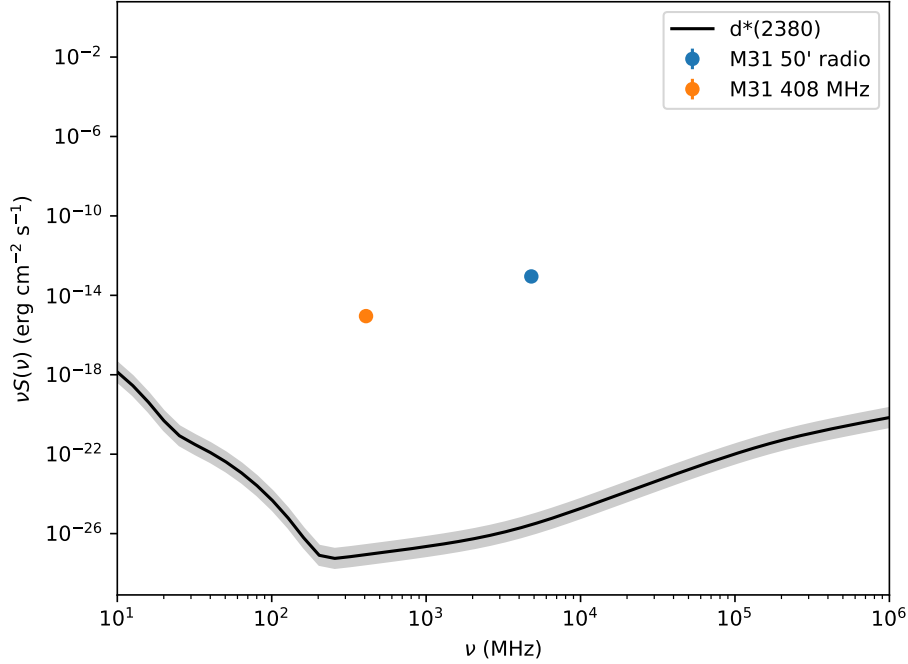


Figure 2. Predicted radio spectrum from d^* decay in the M31 galaxy within $50'$ with $\Gamma_{d^*} = 10^{-24} \text{ s}^{-1}$. The shaded region indicates uncertainties from the magnetic field and halo mass.

galactic emissions to constrain decaying DM models both via direct decay to photons and from final state radiation. Due to the differences with the hexaquark model we compare to a modified model-translated limit of 10^{-19} s^{-1} . The most optimistic observation case is from our results is the Milky-Way galactic centre which produces limits from gamma-ray fluxes similar to model-independent limits from [7] and 5 orders of magnitude better than the roughly translated value 10^{-19} s^{-1} . Despite being two orders of magnitude smaller than Γ_{d^*} limits from the galactic centre, M31 and Coma still provide limits $\Gamma_{d^*} \lesssim 10^{-22} \text{ s}^{-1}$, indicating a particle lifetime lower limit around two orders of magnitude in excess of the age of the universe. If not for the limited energy range of the Reticulum II gamma-ray data it is likely that the strongest extra-galactic environment for these constraints is dwarf galaxies (particularly with gamma-ray measurements or perhaps millimetre telescopes). Radio limits are weak across the board due to the very low energy of the synchrotron peak as a consequence of the small d^* mass. Particularly, this synchrotron peak lies below 10 MHz and is therefore likely unobservable within the atmosphere of Earth.

The uncertainties from halo parameters in the displayed results are notably small in comparison to the difference with the lower limits from [7] and tend to be smaller in the simpler gamma-ray region of the spectrum. However, unquantified uncertainties exist in terms of the required Γ value to achieve a significant present-day DM fraction and in the formalism used to convert charged pion products to electrons/positrons (as

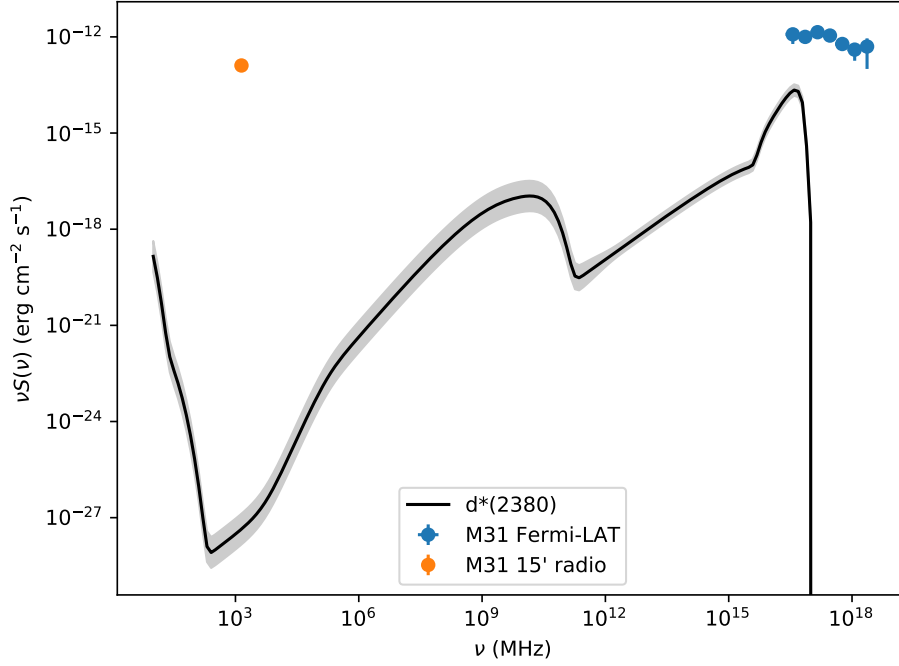


Figure 3. Predicted multi-frequency spectrum from d^* decay in the M31 galaxy within 15' with $\Gamma_{d^*} = 10^{-24} \text{ s}^{-1}$. The shaded region indicates uncertainties from the magnetic field and halo mass.

the quantitative effect of the neglected radiative corrections is unknown). This latter uncertainty does not affect the gamma-ray results as they were all attained from the pion decay channels of d^* .

Despite these uncertainties it seems likely that the emissions from d^* hexquark decay produce relatively weak fluxes in astrophysical environments but that gamma-ray searches in galaxy clusters, galaxies, and dwarf galaxies at energies below 1 GeV may be able to provide further constraints. The most promising target being our own galactic centre whose Fermi-LAT excess constraint betters the existing results derived for model independent cases. The data used in this work was not optimised for this kind of indirect DM search so the results produced could undoubtedly be improved upon in the future.

Acknowledgements

G.B acknowledges support from a National Research Foundation of South Africa Thuthuka grant no. 117969. This research has made use of the NASA/IPAC Extragalactic Database (NED), which is operated by the Jet Propulsion Laboratory, California Institute of Technology, under contract with the National Aeronautics and Space Administration. This work also made use of the WebPlotDigitizer[‡].

[1] Bertone G and Tait Tim M P 2018 *Nature* **562** 51–56 (*Preprint* 1810.01668)

[‡] <http://automeris.io/WebPlotDigitizer/>

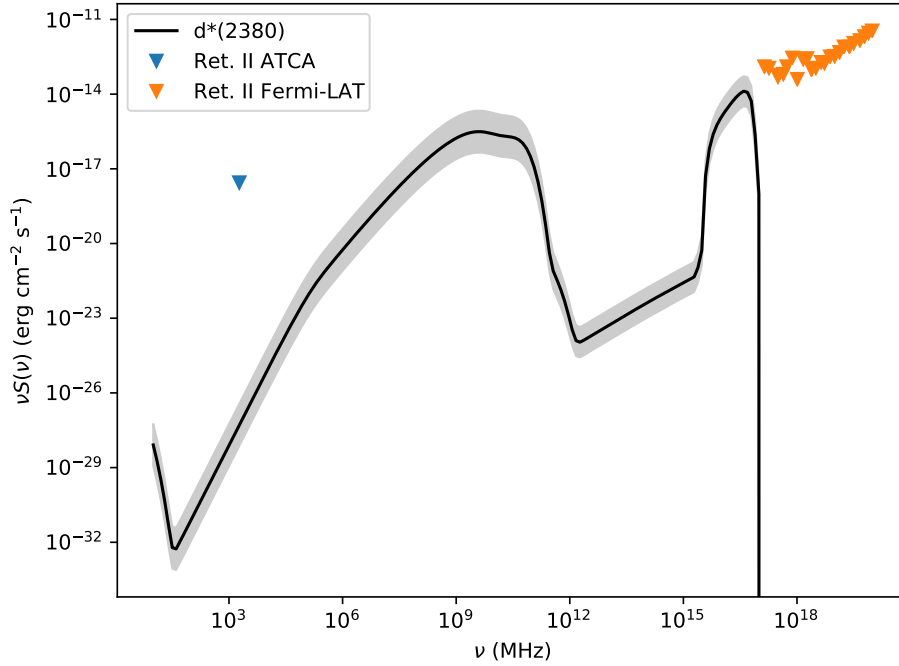


Figure 4. Predicted multi-frequency spectrum from d^* decay in the Reticulum II dwarf galaxy within $30'$ with $\Gamma_{d^*} = 10^{-24} \text{ s}^{-1}$. The shaded region indicates uncertainties from the magnetic field and halo mass.

- [2] Aprile E *et al.* (XENON Collaboration 7) 2018 *Phys. Rev. Lett.* **121**(11) 111302 URL <https://link.aps.org/doi/10.1103/PhysRevLett.121.111302>
- [3] Ackermann M *et al.* (Fermi-LAT Collaboration) 2016 *The Astrophysical Journal* **819** 149 ISSN 1538-4357 URL <http://dx.doi.org/10.3847/0004-637X/819/2/149>
- [4] Albert A *et al.* (Fermi-LAT and DES Collaborations) 2017 *The Astrophysical Journal* **834** 110 ISSN 1538-4357 URL <http://dx.doi.org/10.3847/1538-4357/834/2/110>
- [5] Bashkanov M and Watts D P 2020 *Journal of Physics G: Nuclear and Particle Physics* **47** 03LT01 URL <https://doi.org/10.1088%2F1361-6471%2F67e8>
- [6] Aghanim N *et al.* (Planck Collaboration) 2018 (*Preprint* 1807.06209)
- [7] Essig R, Kuflik E, McDermott S D, Volansky T and Zurek K M 2013 *JHEP* **11** 193 (*Preprint* 1309.4091)
- [8] Scanlon J H and Milford S N 1965 *ApJ* **141** 718
- [9] Longair M S 1994 *High Energy Astrophysics* (Cambridge University Press)
- [10] Rybicki G B and Lightman A P 1986 *Radiative Processes in Astrophysics* (Wiley)
- [11] Colafrancesco S, Profumo S and Ullio P 2006 *A&A* **455** 21
- [12] Egorov A E and Pierpaoli E 2013 *Phys. Rev. D* **88** 023504 (*Preprint* 1304.0517)
- [13] Baltz E A and Edsjö J 1998 *Phys. Rev. D* **59**(2) 023511 URL <https://link.aps.org/doi/10.1103/PhysRevD.59.023511>
- [14] Baltz E A and Wai L 2004 *Phys. Rev. D* **70**(2) 023512 URL <https://link.aps.org/doi/10.1103/PhysRevD.70.023512>
- [15] Beck G 2019 *JCAP* **1908** 019 (*Preprint* 1905.05599)
- [16] Navarro J F, Frenk C S and White S D M 1996 *Astrophys. J.* **462** 563–575 (*Preprint* astro-ph/9508025)
- [17] Burkert A 1996 *IAU Symp.* **171** 175 [*Astrophys. J.*447,L25(1995)] (*Preprint* astro-ph/9504041)
- [18] Briel U G, Henry J P and Boehringer H 1992 *Astronomy and Astrophysics* **259** L31–L34

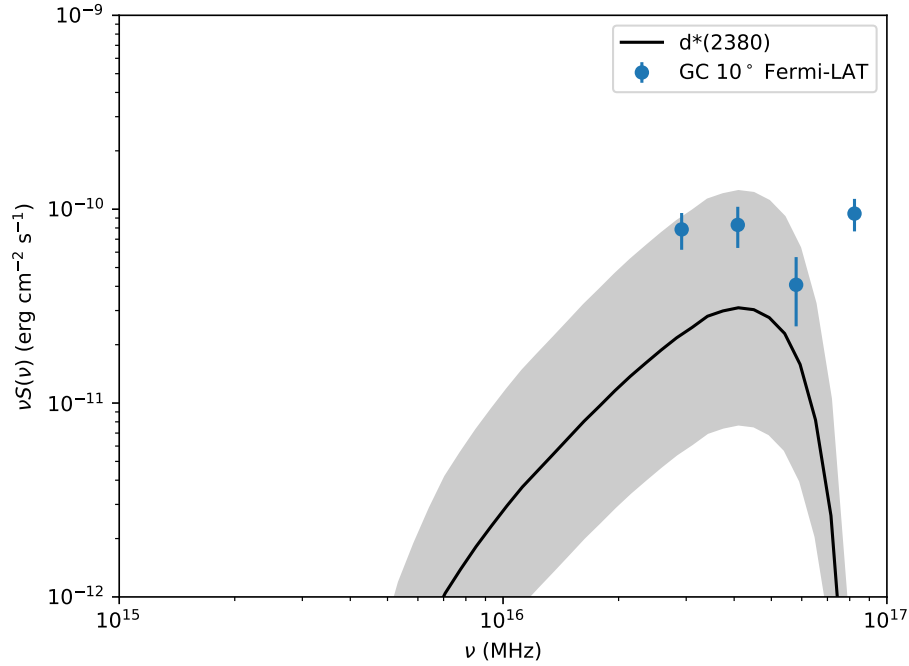


Figure 5. Predicted multi-frequency spectrum from d^* decay within 10° of the Milky-Way galactic centre with $\Gamma_{d^*} = 10^{-24} \text{ s}^{-1}$. The shaded region indicates uncertainties from the halo J-factor.

- [19] Bonafede A, Feretti L, Murgia M, Govoni F, Giovannini G, Dallacasa D, Dolag K and Taylor G B 2010 *Astronomy and Astrophysics* **513** A30 ISSN 1432-0746 URL <http://dx.doi.org/10.1051/0004-6361/200913696>
- [20] Tamm A, Tempel E, Tenjes P, Tihhonova O and Tuvikene T 2012 *A&A* **546** A4 (*Preprint* 1208.5712)
- [21] Beck R 1982 *A&A* **106** 121
- [22] Ruiz-Granados B, Rubiño-Martín J A, Florido E and Battaner E 2010 *ApJ* **723** L44–L48 URL <https://doi.org/10.1088%2F2041-8205%2F723%2F1%2F144>
- [23] Walker M G, Mateo M, Olszewski E W, narrubia J P, Evans N W and Gilmore G 2009 *ApJ* **704** 1274 URL <http://stacks.iop.org/0004-637X/704/i=2/a=1274>
- [24] Adams J J *et al.* 2014 *ApJ* **789** 63 URL <http://stacks.iop.org/0004-637X/789/i=1/a=63>
- [25] Regis M, Richter L and Colafrancesco S 2017 *Journal of Cosmology and Astroparticle Physics* **2017** 025 URL <http://stacks.iop.org/1475-7516/2017/i=07/a=025>
- [26] Bechtol K *et al.* (DES Collaboration) 2015 *ApJ* **807** 50 (*Preprint* 1503.02584)
- [27] Koposov S E, Belokurov V, Torrealba G and Evans N W 2015 *ApJ* **805** 130 (*Preprint* 1503.02079)
- [28] Charbonnier A, Combet C and Maurin D 2012 *Computer Physics Communications* **183** 656668 ISSN 0010-4655 URL <http://dx.doi.org/10.1016/j.cpc.2011.10.017>
- [29] Bonnivard V, Htten M, Nezri E, Charbonnier A, Combet C and Maurin D 2016 *Computer Physics Communications* **200** 336349 ISSN 0010-4655 URL <http://dx.doi.org/10.1016/j.cpc.2015.11.012>
- [30] Hütten M, Combet C and Maurin D 2019 *Computer Physics Communications* **235** 336–345 (*Preprint* 1806.08639)
- [31] Einasto J 1968 *Publications of the Tartuskoj Astrofizika Observatory* **36** 414
- [32] Thierbach M, Klein U and Wielebinski R 2003 *A&A* **397** 53
- [33] Ackermann M *et al.* (Fermi-LAT Collaboration) 2017 *The Astrophysical Journal* **836** 208 URL

<https://doi.org/10.3847/2F1538-4357/2Faa5c3d>

- [34] Ackermann M, Ajello M, Albert A, Atwood W B, Baldini L, Ballet J, Barbiellini G, Bastieri D, Bellazzini R, Bissaldi E and et al 2017 *The Astrophysical Journal* **840** 43 ISSN 1538-4357 URL <http://dx.doi.org/10.3847/1538-4357/aa6cab>